Environmental Science & Technology

pubs.acs.org/est

Article

Selective Ru Adsorption on SnO_2/CeO_2 Mixed Oxides for Efficient Destruction of Multicomponent Volatile Organic Compounds: From Laboratory to Practical Possibility

Yunpeng Long, Qingjie Meng, Meiling Chen, Xueqing Luo, Qiguang Dai,* Hanfeng Lu, Zhongbiao Wu, and Xiaole Weng*

Cite This: *Environ. Sci. Technol.* 2022, 56, 9762−9772

Read Online

ACCESS | Metrics & More | Article Recommendations | Supporting Information

ABSTRACT: Ru-based catalysts have been extensively employed for the catalytic destruction of chlorinated volatile organic compounds (VOCs), but their versatility for other routine VOCs' destruction has been less explored. Herein, we show that Ru-decorated SnO_2/CeO_2 mixed oxides can sustain H_2O and HCl poisonings and are endowed with extraordinary versatility for a wide range of VOCs' destruction. Selective adsorption of Ru on the cassiterite SnO_2 and CeO_2 nanorods through a Coulomb force can rationally tune the oxidation and dechlorination centers on decorated catalysts, where the epitaxial growth of RuO_x on top of SnO_2 is endowed with excellent dechlorination ability and that on CeO_2 is functional as an oxidation center; the latter could also activate H_2O to provide sufficient H protons for HCl formation. Our developed $Ru/SnO_2/CeO_2$ catalyst can steadily destruct monochlorobenzene, ortho-dichlorobenzene, trichloroethylene, dichloromethane, epichlorohydrin, *N*-hexane, ethyl acetate, toluene, and their mixtures at an optimum temperature of 300 °C, and its monolithic form is also functional at this temperature with few dioxins being detected in the off-gas. Our results imply that the Ru-decorated SnO_2/CeO_2 catalyst can meet the demands of regenerative catalytic oxidation for the treatment of a wide range of VOCs from industrial exhausts.

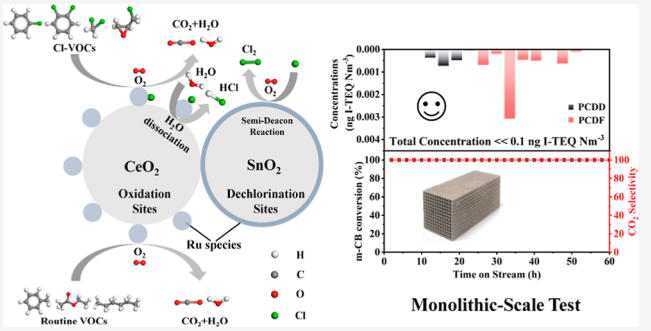

KEYWORDS: *volatile organic compounds, chlorine, versatility, catalytic destruction, catalysis*

1. INTRODUCTION

Industrial emissions of volatile organic compounds (VOCs) are characterized by multicomponent pollutants, wide-range fluctuations, and impurity interferences.[1] Given such a complex operating condition, catalytic combustion usually faces inappropriate pollutant conversion and severe catalyst poisoning, particularly in the presence of chlorinated VOCs (Cl−VOCs).[2] The dissociated Cl is inclined to attack active centers, which causes catalyst deactivation and induces electrophilic chlorination forming toxic polychlorinated byproducts, particularly dioxins.[3] Accordingly, recent efforts for the catalytic combustion of Cl−VOCs have been devoted to designing efficient catalysts with less secondary pollution and more reliable stability.[4−9] However, considering that the vast majority of industrial waste gases usually involve multicomponent VOCs with only trace amounts of Cl−VOCs, developments of versatile catalysts that can sustain Cl attacks and adapt to a wide range of VOCs' destruction are highly demanded.[10,11]

Previously, our group has shown that active phases, for example, Pt, V, Ru, Ce, and Mn, can all generate dioxins in the catalytic destruction of mono-chlorobenzene (m-CB) under laboratory conditions.[3] These toxic byproducts are formed mainly via electrophilic chlorination owing to the inefficient removal of dissociated Cl from Lewis acidic centers.[12] Therefore, further modifications are conducted to sweep the Cl species timely from the catalyst surface, and Brønsted PO_4^{3-}, H-zeolite, WO_3, MoO_3, and VO_x have been extensively employed as the dechlorination center in many state-of-the-art catalysts.[4,5,8−10,13−18] However, introduction of the Brønsted acid sites can inevitably decline the catalyst oxidation ability, and their hydrophilic characteristic is inclined to suppress the H_2O resistance for modified catalysts.[19,20]

Another approach for the efficient removal of Cl species is through a so-called semi-Deacon reaction ($Cl^- + O_2 \rightarrow Cl^\bullet + O^{2-}$), and Ru-based catalysts, particularly Ru/CeO_2, have been widely investigated.[3,21−23] The Ru catalysts were first

Received: April 25, 2022
Revised: June 9, 2022
Accepted: June 14, 2022
Published: June 23, 2022

introduced by Shell Company in the 1960s to recover hydrogen chloride into chlorine (i.e., Deacon reaction: HCl + O_2 → Cl_2 + H_2O),[24] and RuO_2/TiO_2-rutile and RuO_2/SnO_2-cassiterite have been shown with superior activity for this reaction, which are successfully commercialized by Sumitomo and Bayer companies, respectively.[25,26] The Ru catalysts are endowed with extraordinary Cl resistance because their in-depth chlorination can be suppressed by selective and self-limiting surface chlorination[27] and moderate metal−oxygen binding energy, ensuring a high redox ability for the Deacon reaction.[28] Referring to these benefits, we have developed a Ru/Ti−CeO_2 catalyst that exhibited remarkable activity and stability in the catalytic destruction of 1,2-dichloroethane (DCE), trichloroethylene (TCE), and m-CB.[23] Herein, we further show that a Ru-decorated SnO_2/CeO_2 catalyst is also functional for the efficient destruction of Cl−VOCs. In particular, this catalyst is endowed with extraordinary versatility for a wide range of VOCs' destruction. A selective Ru adsorption approach through the Coulomb force was developed, which rationally tuned the oxidation and dechlorination centers between SnO_2 and CeO_2, yielding excellent activity, stability, and H_2O- and HCl-resistances for the catalytic destruction of multicomponent VOCs. Additionally, to carry forward industrial applications, a monolithic catalyst through the honeycomb ceramic coating of Ru catalysts was also developed. Our work illustrates the efforts in transferring theoretical basis into realistic possibility and can guide the design and engineering of versatile catalysts for the efficient catalytic destruction of multicomponent VOCs from industrial exhausts.

2. MATERIALS AND METHODS

2.1. Catalyst Preparation. *2.1.1. Syntheses of CeO_2 Nanorods and Cassiterite SnO_2.* CeO_2 nanorods were fabricated following previous works.[13,29] Briefly, 1.736 g of $Ce(NO)_3{\cdot}6H_2O$ and 19.2 g of NaOH were dissolved in 10 and 70 mL of deionized water, respectively, which were mixed and continuously stirred for 30 min. The solution was then transferred into a Teflon-lined stainless-steel autoclave and hydrothermally treated at 100 °C for 24 h to form CeO_2 nanorods. The formed solids were recovered by centrifugation and washed with deionized water and ethanol several times (until the solution was neutral) and then dried at 100 °C for 12 h. Cassiterite SnO_2 were synthesized also following a previously reported method.[30] Briefly, 2.26 g of $SnCl_2{\cdot}2H_2O$ and 0.08 g of NaOH were milled for 15 min and mixed with 3.57 g of NaCl. Thereafter, the mixture was ground for another 15 min and was calcined at 400 °C for 2 h in air to form SnO_2. Finally, the products were washed with deionized water (3*500 mL) and dried at 60 °C for 8 h.

2.1.2. Selective Ru Adsorption on SnO_2/CeO_2 Mixed Oxides. Selective Ru adsorption was achieved via a wet impregnation route assisted by the Coulomb force. The potential of zero charges (PZC) of as-prepared CeO_2 nanorods and cassiterite SnO_2 were measured at 6.8 and 4.8, respectively (see Supporting Information Figure S1). Therefore, pH values of 5.8 and 8.0 were selected to regulate the Ru adsorptions between CeO_2 and SnO_2. The SnO_2/CeO_2 mixed oxides were fabricated by mixing 9.0 g of CeO_2 nanorods and 1.0 g of cassiterite SnO_2 in a ball grinder with a stirring rate of 250 rpm for 10 h. For the fabrication of the $Ru/SnO_2/CeO_2$ catalyst at pH = 8.0, 4.0 g of SnO_2/CeO_2 mixed oxide was added in 100 mL of deionized water and the temperature was maintained at 50 °C. Thereafter, $RuCl_3$ solution (the amount of Ru was 0.04 g) was added with the pH adjusted to 8.0 by using 0.1 mol/L HCl or 0.1 mol/L NaOH. The mixture was then stirred at 50 °C for 1 h, washed with deionized water, dried at 80 °C for 10 h, and calcined at 350 °C for 3 h. The obtained product is hereafter denoted as Ru/SnCe-(8.0). Other samples, for example, Ru/SnCe-(5.8), Ru/Sn-(5.8), and Ru/Ce-(8.0), were prepared following the same procedure, except for their supports and pH values.

2.1.3. Honeycomb Ceramic Coating. Briefly, 6.0 g of silica sol (30% SiO_2, pH: 2.2−3.6), 12.0 g of Ru/SnCe-(5.8) powder, and 30 mL of H_2O were continually stirred at 25 °C for 8 h to obtain a coating solution. Cordierite honey ceramic (i.e., cordierite) was cut into cuboids (22 mm*22 mm*50 mm), dipped into the coating solution, and the excess solution was bowed off with high-purity air. After 12 h of natural drying at room temperature, the coating of the sample was repeated two more times, which was then dried at 60 °C for 3 h, and calcined at 450 °C for 2 h with a heating rate of 5 °C/min. The obtained product is hereafter denoted as Ru/SnCe-(5.8, Honeycomb). The mass fraction of Ru/SnCe-(5.8) powder in Ru/SnCe-(5.8, Honeycomb) was measured at approximately 10.0%.

2.2. Catalyst Characterization and Activity Measurements. The structural and physicochemical properties of as-prepared samples were analyzed by using a range of analytical techniques. Details are illustrated in the Supporting Information. The catalytic activity was measured in a continuous fixed-bed quartz reactor (i.d. = 4 mm) with a thermocouple of K-type with a programmable temperature controller at the center to accurately measure the reaction temperature. During the measurements, 0.3 g of the powder sample with a 40−60 mesh was loaded into the quartz reactor. The simulated gas mixture consisted of 500 ppm m-CB (a typical Cl−VOCs) and/or other typical VOCs, 45 mL min^{-1} N_2, and 5 mL min^{-1} O_2. The total flow rate of the mixed reactant gas was set at 50 mL·min^{-1} with the weight hour space velocity (WHSV) at approximately 10,000 mL g^{-1} h^{-1}. Liquid-phase VOCs were injected into a vaporizer with a peristaltic pump. All the pipelines were electrically heated to ensure complete evaporation. The reactants and products were analyzed using a gas chromatograph (Agilent Technologies 7890A GC, Agilent technologies Inc., USA) equipped with a thermal conduction detector and a flame ionization detector. Reaction temperatures were controlled over the range 100−300 °C. Activity measurement errors were controlled to lower than 3%. Apparent activation energies (E_a) were measured by using an Arrhenius equation. Details are given in the Supporting Information.

The catalytic performance at the monolithic-scale test determines the application from lab to practice. Briefly, the Ru/SnCe-(5.8, Honeycomb) catalyst was fixed in a steel tube. We used fiberglass tape to wrap the ceramic body in order to prevent gas from escaping around. Feed gas was composed of impressed indoor air and thermally vaporized m-CB. The m-CB concentration was 500 ppm and the flowing rate was 350 mL/min. Based on the actual mass of powder loading, the WHSV was calculated at approximately 15,000 mL g^{-1} h^{-1}. Local atmospheric pressure, relative humidity, and temperature were recorded hourly to calculate the absolute humidity in the feed gas during the monolithic-scale test.

https://doi.org/10.1021/acs.est.2c02925
Environ. Sci. Technol. 2022, 56, 9762−9772

Table 1. Elemental Analyses, m-CB Conversion Efficiencies (T_{50}/T_{90}), Reaction Rates at 160 °C, Activation Energies (E_a), and Ru Dispersion Rates for Ru-Decorated Samples

sample	Ru/SnCe-(8.0)	Ru/SnCe-(5.8)	Ru/Sn-(5.8)	Ru/Ce-(8.0)
Ru[a] (wt %)	0.88%	0.91%	0.97%	0.90%
SnO_2[a] (wt %)	8.39%	9.16%	99.03%	
CeO_2[a] (wt %)	90.73%	89.93%		99.10%
T_{50}/T_{90}[b](°C)	132/167	127/166	224/257	140/170
T_{50}/T_{90}[c](°C)	267/312	209/280	279/306	262/312
$k_{160°C}$[c](mol·s^{-1} g^{-1})	4.54 × 10^{-5}	5.81 × 10^{-5}	2.22 × 10^{-5}	2.48 × 10^{-5}
E_a[d](kJ/mol)	31.68	28.99	78.92	47.57
Ru dispersion[e]	6.23%	13.59%	8.32%	3.27%

[a]By XRF. [b]At 10,000 mL g^{-1} h^{-1} WHSV. [c]At 60,000 mL g^{-1} h^{-1} WHSV. [d]By the Arrhenius equation at 60,000 mL g^{-1} h^{-1} WHSV. [e]By H_2 pulse chemisorption.

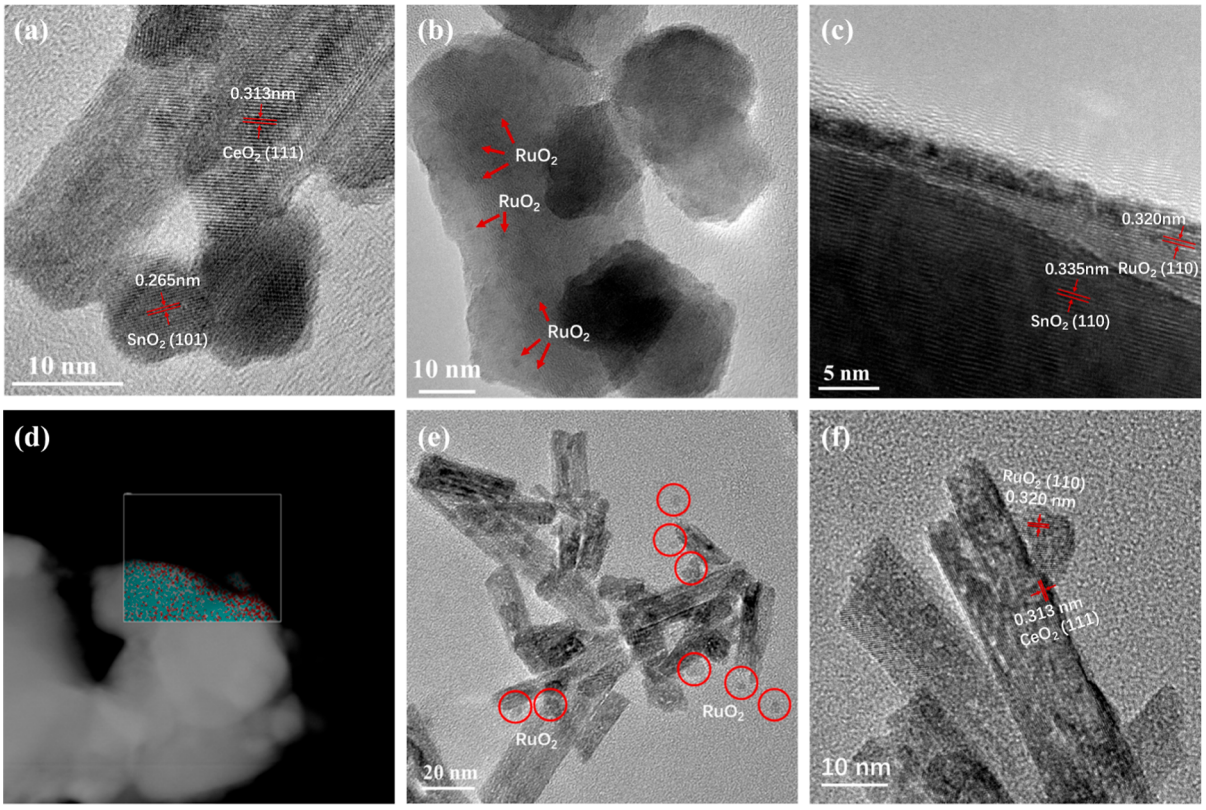

Figure 1. (a–c) HRTEM images and (d) EDX-mapping of the Ru/SnCe-(5.8) sample (red: Ru element; cyan: Sn element); (e,f) HRTEM images of the Ru/SnCe-(8.0) sample.

3. RESULTS AND DISCUSSION

3.1. Textural Analyses on As-Prepared Samples. Phase identity and purity of as-prepared samples were analyzed using X-ray powder diffraction. As shown in Supporting Information Figures S2, S3, all samples exhibited their corresponding characteristic peaks for CeO_2 (JCPDS no. 43-1002) and/or cassiterite SnO_2 (JCPDS no. 41-1445). The diffraction peaks for CeO_2 in the SnO_2/CeO_2 mixed oxide were slightly shifted to a higher 2θ range, suggesting a shrink of the CeO_2 lattice as induced by the Sn partial dopant because the incorporation of a lower atomic radius Sn (1.41 Å) would cause the lattice shrink of CeO_2 (atomic radius Ce = 1.83 Å). Selective adsorption of Ru on the SnO_2/CeO_2 mixed oxides did not yield any characteristic peaks for Ru species, which could be ascribed to their low contents (≤1.0 wt %). Brunner–Emmet–Teller (BET) surface area measurements (Supporting Information Table S1) revealed that CeO_2 and cassiterite SnO_2 had S_{BET} values of 116.2 and 14.1 m^2 g^{-1}, respectively, where their dry-mixing yielded a S_{BET} value of 90.6 m^2 g^{-1}. The loadings of Ru seemed not to distinctly change the S_{BET}, and all samples displayed a type IV N_2 adsorption–desorption isotherm with a H_3-type hysteresis loop in the relative pressure (P/P_0) range of 0.1–1.0 (Supporting Information Figure S4 and Table S1), indicating the characteristics of mesoporous structures and the existence of slit pores (originating from particles stacking).[7] X-ray fluorescence (XRF) analyses confirmed approximately 0.88–0.97% Ru in weight for each sample (see Table 1), which were relatively consistent with their theoretical values.

3.2. Confirmation of Selective Ru Adsorption on SnO_2/CeO_2 Mixed Oxides. According to the PZC values as measured for CeO_2 (PZC = 6.8) and cassiterite SnO_2 (PZC = 4.8), we expected that under pH = 8, the Ru species should randomly adsorb on CeO_2 and SnO_2 surfaces owing to their

https://doi.org/10.1021/acs.est.2c02925
Environ. Sci. Technol. 2022, 56, 9762–9772

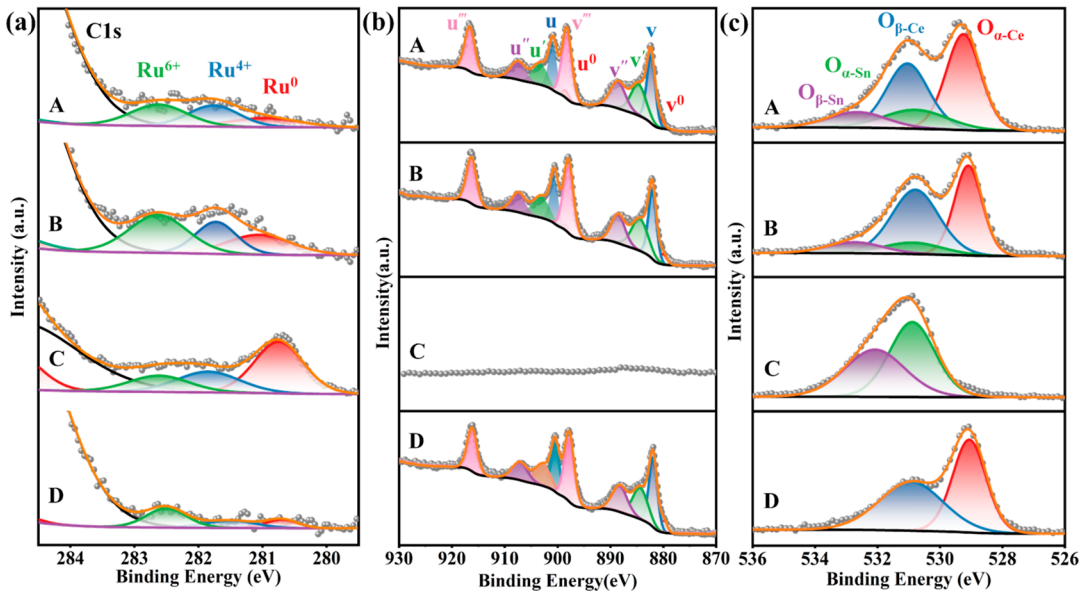

Figure 2. (a) Ru 3d, (b) Ce 3d, and (c) O 1s XPS profiles of Ru-decorated samples: (A) Ru/SnCe-(8.0), (B) Ru/SnCe-(5.8), (C) Ru/Sn-(5.8), and (D) Ru/Ce-(8.0).

surficial negative charges, while at pH = 5.8, they should preferentially adsorb on the SnO_2 surface. To verify this adsorption feature, high-resolution transmission electron microscopy (HRTEM) was employed. As shown in Figure 1, both the Ru-decorated samples under pH = 8 and pH = 5.8 exhibited corresponding lattice spacings of 0.313 nm for the (111) plane of CeO_2 nanorods and 0.265 nm for the (101) plane of cassiterite SnO_2. The Ru/SnCe-(5.8) was shown with significant fine Ru species on the SnO_2 surface (Figure 1b), with an epitaxial growth of the RuO_2 film on top of SnO_2 originating from their lattice matching (Figure 1c,d).[31] In comparison, the Ru/SnCe-(8.0) sample revealed distinct RuO_x particles, with the corresponding lattice spacing of 0.320 nm for the (110) plane on CeO_2 nanorods (Figure 1e,f). We assumed that the film form of RuO_2 on SnO_2 could induce superior Ru surficial dispersion on the oxide supports. Indeed, after being subjected to H_2 pulse chemisorption measurements (see Table 1), Ru/Sn-(5.8) revealed a Ru dispersion rate of approximately 8.32%, which is nearly twofold higher than that of Ru/Ce-(8.0) (approximately 3.27%). Similar results were also observed in Ru/SnCe-(5.8) and Ru/SnCe-(8.0) samples. The distinctly varied Ru dispersion and their HRTEM observations both verify our expectation that Ru/SnCe-(5.8) was with more Ru on SnO_2 than Ru/SnCe-(8.0).

3.3. X-Ray Photoelectron Spectroscopy Analyses. X-ray photoelectron spectroscopy (XPS) was employed for further confirming such an adsorption feature of Ru. As shown in Supporting Information Figure S5a and Table S2, full-scans of XPS indicated the existence of Ru, Ce, and Sn elements on corresponding samples. Among the investigated samples, the Ru/Ce-(8.0) sample exhibited the lowest surficial Ru content (at 0.37 at %), which could be ascribed to its low Ru dispersion as verified by the H_2 pulse chemisorption measurements (see Table 1).

In the SnO_2/CeO_2 mixed oxide, the binding energy (BE) of Sn 3d XPS was shown to shift to a higher BE range (see Supporting Information Figure S6) and those in Ce 3d XPS shifted to a lower BE range. This further confirmed their mutual interaction by drying mixing and was consistent with the XRD results (see Supporting Information Figure S2). The Ru-decorated samples displayed Ru $3d_{5/2}$ peaks at 280.8, 218.5, and 282.8 eV, which were ascribed to Ru^0, Ru^{4+}, and Ru^{6+}, respectively (Figure 2a).[32,33] As shown in Supporting Information Table S2, the Ru/Sn-(5.8) sample exhibited the majority of the Ru^0 chemical state with approximately 52.46% of the total Ru, the origin of which could be ascribed to the electron transfer from Sn (electronegativity at 1.96) to Ru (electronegativity at 2.2)[34,35] In contrast, the Ru/Ce-(8.0) sample exhibited less intense Ru $3d_{5/2}$ peaks (owing to the low content of surficial Ru) and revealed the majority of Ru^{6+} chemical state with approximately 55.05% of the total Ru. This was unsurprising given the mutual interaction between Ru and CeO_2 that could cause the transformation of Ce^{4+} to Ce^{3+}, leading to the loss of electrons from Ru[36,37] (see Ce 3d XPS in Supporting Information Figure S6). However, for Ru-decorated mixed oxides, the Ru/SnCe-(5.8) sample yielded approximately 26.64% Ru^0, which was comparatively higher than that of Ru/SnCe-(8.0) (at 21.37%). This further verified that Ru/SnCe-(5.8) was with more Ru on SnO_2 and was consistent with the HRTEM results. Considering that the overlap between C 1s and Ru 3d peaks might cause the XPS results dependent on peak deconvolutions, Ru 3p profiles were also analyzed. As shown in Supporting Information Table S2 and Figure S5b, similar amounts of Ru valence states in the corresponding samples were observed, confirming the validity of Ru 3d assignments.

However, for Ce 3d XPS, the Ce^{3+} chemical state corresponded to v^0 (880.5 eV), v' (884.7 eV), u^0 (898.5 eV), and u' (903.2 eV) peaks, and Ce^{4+} was assigned to v (882.3 eV), v'' (888.6 eV), v''' (898.2 eV), u (900.9 eV), u'' (907.5 eV), and u''' (916.6 eV) peaks (Figure 2b).[38,39] As shown in Supporting Information Table S2, the Ru/SnCe-(5.8) sample yielded a Ce^{3+} content at a $Ce^{3+}/(Ce^{3+} + Ce^{4+})$ molar ratio of approximately 27.14%, while Ru/SnCe-(8.0) was at approximately 24.70%. For the O 1s XPS, the peak at 529.3 eV was ascribed to lattice oxygen of CeO_2 ($O_{\alpha\text{-Ce}}$) and that at 531.1 eV belonged to surficial chemisorbed oxygen of CeO_2 ($O_{\beta\text{-Ce}}$). The peak at 530.8 eV corresponded to the

https://doi.org/10.1021/acs.est.2c02925
Environ. Sci. Technol. 2022, 56, 9762−9772

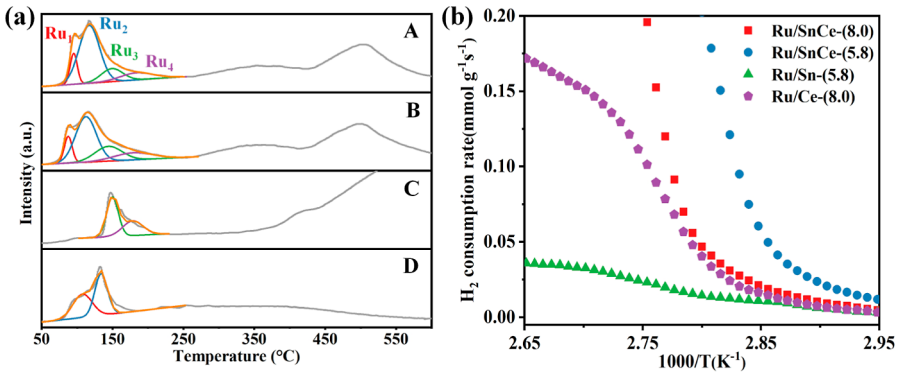

Figure 3. (a) H_2-TPR profiles of Ru-decorated catalysts and (b) initial H_2 consumption rate plots derived from H_2-TPR profiles. (A) Ru/SnCe-(8.0), (B) Ru/SnCe-(5.8), (C) Ru/Sn-(5.8), and (D) Ru/Ce-(8.0).

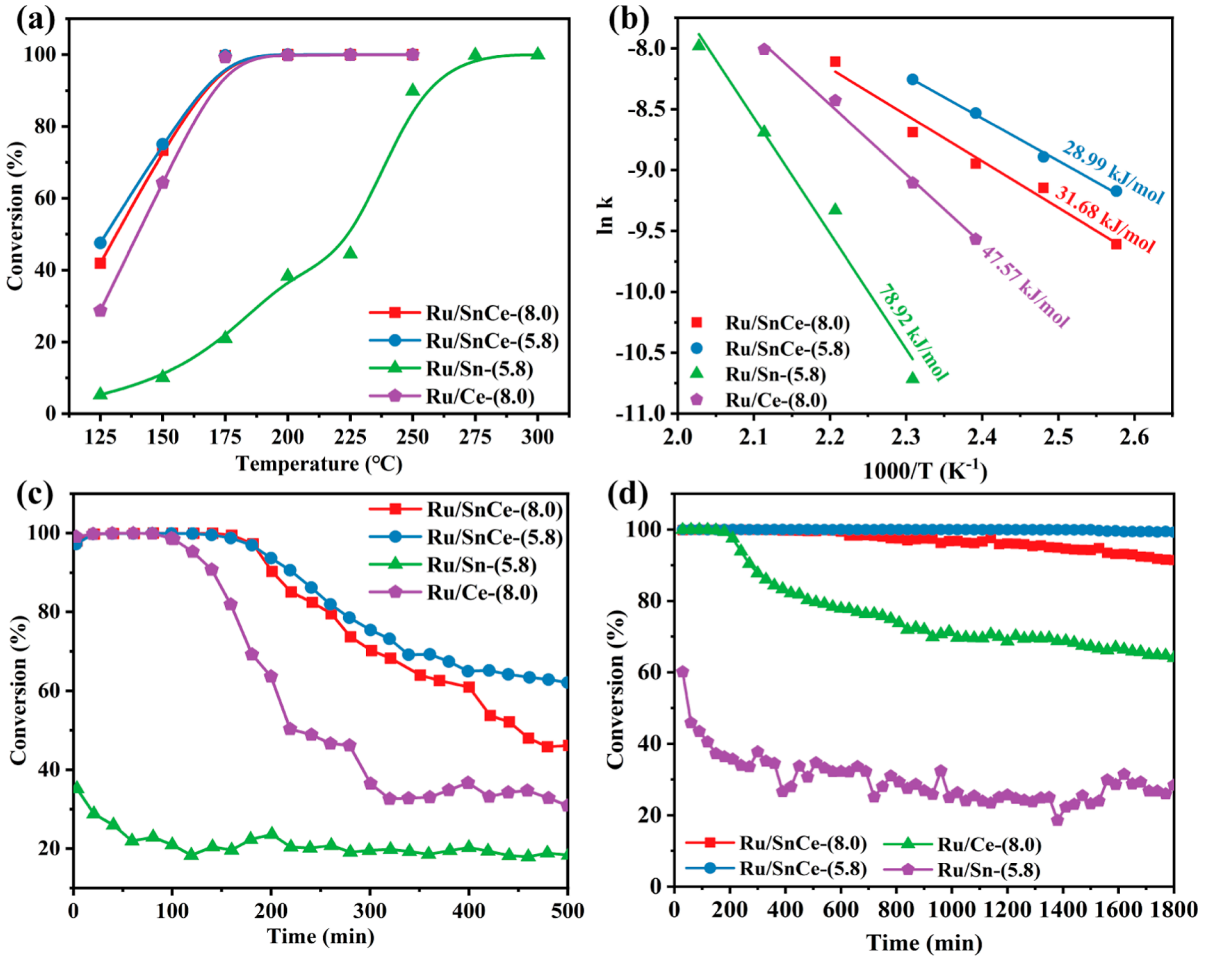

Figure 4. (a) Light-off curves of m-CB destruction over Ru-decorated samples (500 ppm m-CB, 10% O_2, N_2 balance gas, WHSV = 10,000 mL g^{-1} h^{-1}); (b) Arrhenius plots for the catalytic destruction of m-CB over Ru-decorated samples (500 ppm m-CB, 10% O_2, N_2 balance gas, WHSV = 60,000 mL g^{-1} h^{-1}); (c) durability tests at 225 °C and (d) durability tests at 250 °C for Ru-decorated samples (500 ppm m-CB, 10% O_2, N_2 balance gas, WHSV = 10,000 mL g^{-1} h^{-1}).

lattice oxygen of SnO_2 ($O_{\alpha\text{-Sn}}$) and that at 532.6 eV was ascribed to surficial chemisorbed oxygen of SnO_2 ($O_{\beta\text{-Sn}}$) (Figure 2c).[32,40] It was noted that the Ru/SnCe-(5.8) sample exhibited the $O_{\beta\text{-Ce}}$ at a molar ratio of 44.50%, which was higher than that in the Ru/SnCe-(8.0) sample (at 33.50%), consistent with their $Ce^{3+}/(Ce^{3+} + Ce^{4+})$ molar ratio in Ce 3d XPS. From the XPS results, we concluded that the variation in pH not only tuned the selective adsorption of Ru on oxide supports but also changed the surface nature of their decorated samples.

3.4. TPR Measurements. To further evaluate the adsorption feature of Ru species and their resulted redox ability for each sample, H_2-temperature programmed reduction (TPR) analyses were performed. As shown in Figure 3a, Ru/Ce-(8.0) exhibited H_2 consumption peaks at approximately 108 and 134 °C, which were ascribed to the reductions of highly dispersed Ru species on CeO_2 (referred to as Ru_1 in

https://doi.org/10.1021/acs.est.2c02925
Environ. Sci. Technol. 2022, 56, 9762−9772

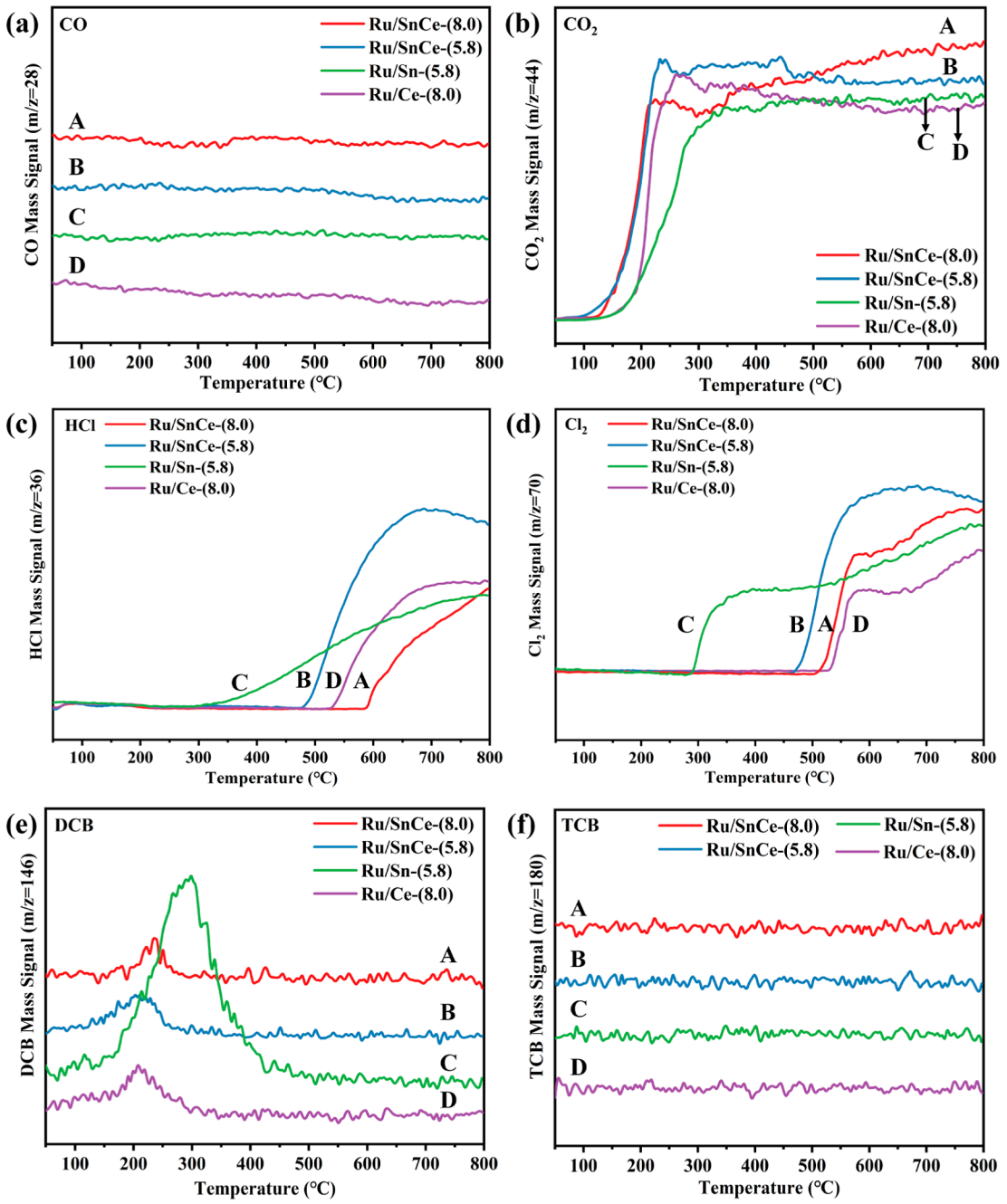

Figure 5. CB-TPSR profiles of Ru-decorated catalysts. (A) Ru/SnCe-(8.0), (B) Ru/SnCe-(5.8), (C) Ru/Sn-(5.8), and (D) Ru/Ce-(8.0).

Supporting Information Table S3) and large RuO_2 particles (Ru_2), respectively.[41] The Ru/Sn-(5.8) sample yielded H_2 consumption peaks at approximately 150 and 179 °C, which corresponded to the reductions of large RuO_2 particles (Ru_3) and highly dispersed Ru species on SnO_2 (Ru_4), respectively.[42] Overlapping peak deconvolution confirmed both the Ru/SnCe-(5.8) and Ru/SnCe-(8.0) samples with the large RuO_2 particles and the Ru species dispersed on CeO_2 and SnO_2, which were consistent with their HRTEM observations (see Figure 1). In particular, we noted that peak areas corresponding to the Ru species dispersed on SnO_2, that is, Ru_3 and Ru_4, were much higher in Ru/SnCe-(5.8) than in Ru/SnCe-(8.0). This further confirmed the more Ru dispersion on SnO_2 in the Ru/SnCe-(5.8) sample, consistent with the HRTEM, XPS, and H_2 pulse chemisorption results.

Furthermore, the Ru/SnCe-(5.8) sample exhibited relatively lower H_2 consumption peaks for Ru_1 and Ru_2 than the Ru/SnCe-(8.0) sample. This indicated that the redox ability of Ru-decorated CeO_2 could be tuned by varying the pH. We assumed that the pH at 5.8 with the positive charges on CeO_2 could induce a higher Ru dispersion than that at 8.0 (with negative charges) because the latter would strongly attract Ru^{3+} precursors, leading to RuO_x accumulation and aggregation at elevated temperatures. To verify this, we fabricated a Ru/Ce-(5.8) sample, while its H_2 consumption peaks for Ru_1 and Ru_2 were both shifted to lower temperatures in comparison with Ru/Ce-(8.0) (see Supporting Information Figure S7), confirming the high dispersion of Ru on the CeO_2 at pH = 5.8. Such an interaction feature between Ru and CeO_2 was also verified by Raman analyses. As shown in Supporting

https://doi.org/10.1021/acs.est.2c02925
Environ. Sci. Technol. 2022, 56, 9762−9772

Information Figure S8, a weak band at approximately 971 cm^{-1} for Ru−O−Ce[43,44] appeared in both Ru/Ce-(8.0) and Ru/SnCe-(8.0) samples. However, this band was absent in the Ru/SnCe-(5.8) sample. Additionally, we had calculated the initial H_2 consumption rates, that is, the consumed H_2 less than 25% for the first reduction peak for each sample, aiming to estimate their low-temperature reducibility.[45] As shown in Figure 3b, the Ru/SnCe-(5.8) sample yielded the highest initial H_2 consumption rate, revealing the best redox ability among investigated samples.

3.5. Catalytic Activity Measurements. Figure 4a shows the light-off curves for the catalytic destruction of m-CB over each sample. Samples were first subjected to a reaction condition with 500 ppm m-CB, 10% O_2, N_2 balance gas, and WHSV = 10,000 mL g^{-1} h^{-1}. The Ru/Sn-(5.8) sample yielded the lowest activity in m-CB conversion, which was unsurprising given its poor redox ability as verified by H_2-TPR analyses (see Figure 3). Other samples exhibited a nearly identical m-CB conversion efficiency, with the T_{90} (i.e., temperature for 90% conversion of m-CB) at approximately 170 °C. However, further kinetic measurements (see Figure 4b and Table 1) under the condition of 500 ppm m-CB, 10% O_2, N_2 balance gas, and WHSV = 60,000 mL g^{-1} h^{-1} indicated that the reaction rate at 160 °C was with the sequence of Ru/SnCe-(5.8) (5.81×10^{-5} mol·s^{-1} g^{-1}) > Ru/SnCe-(8.0) (4.54×10^{-5} mol·s^{-1} g^{-1}) > Ru/Ce-(8.0) (2.48×10^{-5} mol·s^{-1} g^{-1}) > Ru/Sn-(5.8) (2.22×10^{-5} mol·s^{-1} g^{-1}), and their activation energies followed an opposite order: Ru/SnCe-(5.8) (28.99 kJ/mol) < Ru/SnCe-(8.0) (31.68 kJ/mol) < Ru/Ce-(8.0) (47.57 kJ/mol) < Ru/Sn-(5.8) (78.92 kJ/mol). Compared to the state-of-the-art catalysts (see Supporting Information Table S4), Ru/SnCe-(5.8) had yielded the lowest E_a in the catalytic destruction of m-CB.

However, after being subjected to stability tests, all samples were deactivated at 225 °C (see Figure 4c), where the Ru/SnCe-(5.8) sample retained approximately 65% m-CB conversion after 500 min aging, and Ru/SnCe-(8.0) was at approximately 50%. In contrast, Ru/Ce-(8.0) was rapidly deactivated after 100 min of aging and eventually retained the m-CB conversion at only approximately 30%. Importantly, further elevating the aging temperature to 250 °C resulted in a stable performance for the Ru/SnCe-(5.8) sample, which retained the 100% m-CB conversion for the 1800 min durability test (see Figure 4d), while other samples still suffered the deactivation.

3.6. TPSR Measurements. To gain insights into their varied performances in the catalytic destruction of m-CB, m-CB temperature-programmed surface reaction (CB-TPSR) measurements were performed. As shown in Figure 5a,b, all samples generated the majority of CO_2 during the CB-TPSR measurements, with no obvious CO having been detected. The Ru/Sn-(5.8) sample exhibited the highest on-set temperature for CO_2 generation, which was unsurprising given its poor redox ability as verified by H_2-TPR analyses and was consistent with its activity measurement (see Figure 4). The Ru/Ce-(8.0) sample yielded an on-set temperature for CO_2 generation of approximately 200 °C, which was relatively higher than those of Ru/SnCe-(5.8) and Ru/SnCe-(8.0) (at approximately 150 °C), consistent with their H_2-TPR results.

We proposed that the Ru-decorated CeO_2 should be the main oxidation center in Ru/SnCe-(5.8) and Ru/SnCe-(8.0) samples as our additional experiment by mixing the 10 wt % Ru/Sn-(5.8) with CeO_2 nanorods only retained approximately 40% m-CB conversion at 250 °C after 250 min of aging (see Supporting Information Figure S9). However, for the Ru-decorated SnO_2, they were mainly functional as dechlorination centers as the Ru/Sn-(5.8) sample yielded the lowest HCl and Cl_2 on-set desorption temperatures among the investigated samples (see Figure 5c,d). Wang et al. have indicated that the excellent dechlorination ability of Ru/SnO_2 should originate from their high Ru dispersion and strong Ru−SnO_2 interaction, which inhibited the particle agglomeration at elevated temperatures.[42,46] Herein, we further showed that the epitaxial growth of Ru on SnO_2 could also benefit the transformation of dissociated Cl into the Cl radical as Ru/Sn-(5.8) not only yielded the lowest on-set temperature for Cl_2 desorption but also generated the most dichlorobenzenes via the electrophilic chlorination reaction (see Figure 5e). In contrast, both the Ru/SnCe-(5.8) and Ru/SnCe-(8.0) samples did not yield dichlorobenzene byproducts at temperatures higher than 250 °C. This is promising as the dichlorobenzenes have been demonstrated to be the main precursor for dioxin formation in the catalytic destruction of Cl−VOCs, which would transfer into chlorophenols, followed by the consolidation into dioxins.[13,47] Additionally, the trichlorobenzene byproducts were not observed in all samples.

H_2O temperature-programmed desorption (H_2O-TPD) was also conducted to evaluate the origin of H for HCl formation. It has been reported that, in the H_2O-TPD profile, H_2O desorption at the temperatures of 200−350 °C (caused by surface mobile OH recombination) was more than likely the main H proton source for HCl formation in the catalytic destruction of Cl−VOCs.[7,13] As shown in Supporting Information Figure S10, the Ru/Sn-(5.8) sample did not yield distinct H_2O desorption peaks at temperatures of 200−350 °C, but Ru/Ce-(8.0) did. This indicated that H_2O dissociation providing H protons for HCl formation should be mainly taking place on Ru/CeO_2, consistent with Wang et al.'s report.[48] However, by comparing the Ru/SnCe-(5.8) and Ru/SnCe-(8.0) samples, the former yielded significantly higher H_2O desorption peaks than the latter, and peak fitting at 200−350 °C revealed that the peak area in the Ru/SnCe-(5.8) sample was approximately 63.8% higher than that in the Ru/SnCe-(8.0) sample. This is unusual as Ru/SnCe-(8.0) had been demonstrated with more Ru on CeO_2 than Ru/SnCe-(5.8), which should have more H_2O activation sites (i.e., Ru/CeO_2 interface) than the Ru/SnCe-(5.8) sample. Such an inconsistency was not caused by their surface hydrophobicity difference as static contact angle measurements revealed a similar contact angle for the two samples (see Supporting Information Figure S11). We assumed that the difference in H_2O activation behavior between Ru/SnCe-(5.8) and Ru/SnCe-(8.0) samples could be partly caused by their varied Ru dispersion on CeO_2 as verified by H_2-TPR and the H_2O-TPD of Ru/Ce-(5.8) (see Supporting Information Figure S10), while another cause could be related to their different interfacial water structure on the surface, as Raman analyses (see Supporting Information Figure S12) indicated that the vibration of surface water molecules on the Ru/SnCe-(5.8) sample was shifted to a lower range, suggesting that this sample was with a more ordered interfacial water structure, which could facilitate the dissociation of H_2O into a hydroxide radical owing to the decrease in entropy from a thermodynamic perspective.[49,50]

3.7. H_2O- and HCl-Resistance and Versatility Measurements. Since the industrial emissions of VOCs are

https://doi.org/10.1021/acs.est.2c02925
Environ. Sci. Technol. 2022, 56, 9762−9772

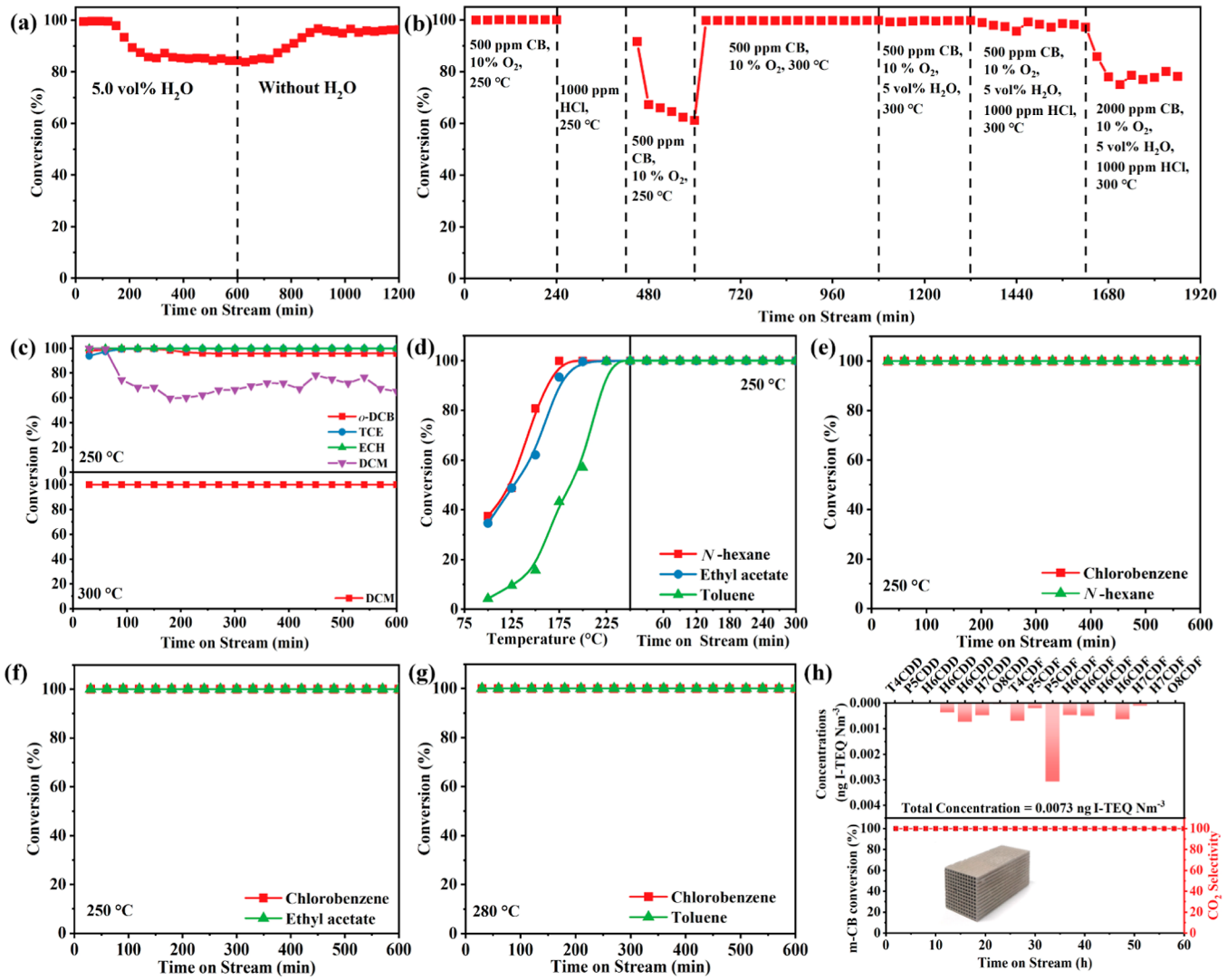

Figure 6. (a) H_2O-resistance of m-CB oxidation over the Ru/SnCe-(5.8) catalyst at 250 °C and (b) H_2O- and HCl-resistance during m-CB oxidation over the Ru/SnCe-(5.8) catalyst (500 ppm m-CB, 10% O_2, 5.0 vol % water vapor when used, N_2 balance gas, and WHSV = 10,000 mL g^{-1} h^{-1}); versatility test of different kinds of (c) Cl−VOCs and (d) routine VOCs over the Ru/SnCe-(5.8) catalyst (500 ppm DCB, TCE, DCM, ECH, *N*-hexane, ethyl acetate, toluene, 10% O_2, N_2 balance gas, and 10,000 mL g^{-1} h^{-1}); durability for catalytic oxidation of the mixed m-CB and (e) *N*-hexane, (f) ethyl acetate, (g) toluene over the Ru/SnCe-(5.8) catalyst (500 ppm m-CB and 500 ppm *N*-hexane/ethyl acetate/toluene, 10% O_2, N_2 balance gas, 10,000 mL g^{-1} h^{-1}, 250, 250, and 280 °C for *N*-hexane, ethyl acetate, and toluene, respectively); (h) durability, CO_2 selectivity, and concentrations of 17 toxic dioxins in the off-gas at 300 °C during m-CB oxidation over Ru/SnCe-(5.8, Honeycomb) catalysts (500 ppm m-CB, indoor air balance gas, and 15,000 mL g^{-1} h^{-1}) (inset: pictures of the monolithic catalyst).

generally with multicomponent pollutants and impurity interferences, H_2O- and HCl-resistance and the versatility of Ru/SnCe-(5.8) were evaluated toward practical applications. As shown in Figure 6a, the introduction of 5 vol % H_2O had induced a slight deactivation in m-CB conversion at 250 °C. However, such a deactivation could be almost recovered after H_2O being switched off, suggesting that the deactivation was caused by the competitive adsorption between H_2O and m-CB.[32,51] Furthermore, corrosive HCl as the final product in the catalytic destruction of Cl−VOCs might destroy the structure of the applied catalysts. Therefore, HCl-resistance of Ru/SnCe-(5.8) was also evaluated. As shown in Figure 6b, Ru/SnCe-(5.8) was first subjected to a 4 h aging at 250 °C, followed by the introduction of 1000 ppm HCl. After 3 h of HCl treatment, a distinct decline in the m-CB conversion from 100 to 60% was observed. However, on further elevating the temperature to 300 °C, the conversion efficiency was mostly recovered, even with the co-existence of 5 vol % H_2O. Furthermore, increasing the m-CB concentration to 2000 ppm had resulted in a decline of m-CB conversion to approximately 70%, but such an efficiency could be retained within the investigated period. Durability measurement results indicated that the Ru/SnCe-(5.8) sample can sustain H_2O and HCl poisonings at elevated temperatures, and an optimum operation temperature for the industrial application of this catalyst is ≥300 °C.

To verify the versatility of Ru/SnCe-(5.8) for other types of Cl−VOCs' destruction, durability tests at 250 °C for ortho-dichlorobenzene (*o*-DCB), TCE, dichloromethane (DCM), and epichlorohydrin (ECH) destruction were conducted. As shown in Figure 6c, all the Cl−VOCs had been steadily destructed at 250 °C, except for DCM, the conversion of which fluctuated at approximately 70%. However, further evaluating the temperature to the optimum 300 °C, DCM

https://doi.org/10.1021/acs.est.2c02925
Environ. Sci. Technol. 2022, 56, 9762−9772

could be steadily destructed. For routine VOCs, for example, *N*-hexane, ethyl acetate, and toluene, all of them were shown to be steadily destructed at 250 °C (see Figure 6d). Even for their mixtures with m-CB, Ru/SnCe-(5.8) still yielded outstanding stability at 250 °C, except for toluene, whose mixture required approximately 280 °C for the steady destruction (see Figure 6g) owing to their competitive adsorption feature, surface chlorination, and steric hindrance effect.[52]

Finally, monolithic Ru/SnCe-(5.8) was fabricated by coating the corresponding powders onto a honeycomb ceramic (22 mm*22 mm*50 mm); details are present in the Section 2.2. A unique binder formula was developed to overcome the hydrophobic Ru coating. The obtained sample was subsequently subjected to a 300 °C durability test under the conditions of 500 ppm m-CB, indoor air balance gas, and WHSV = 15,000 mL g^{-1} h^{-1}. The indoor air was with 28−87% relative humidity at 8−20 °C, which involved approximately 0.53−1.06 vol % H_2O. Durability and CO_2 selectivity of the monolithic Ru/SnCe-(5.8, Honeycomb) are shown in Figure 6h, which shows that m-CB could be steadily destructed at 300 °C for 60 h. In particular, after being subjected to 17 toxic dioxin measurements (see Figure 6h and Supporting Information Table S5), 12 kinds of dioxin homologues in the off-gas were detected. However, the total concentration of these dioxins was measured at only 0.007 ng I-TEQ N m^{-3}, which was far below the national emission standard limit (0.1 ng I-TEQ N m^{-3}). These measurements indicate that Ru/SnCe-(5.8, Honeycomb) can meet the demands of regenerative catalytic oxidation for a wide range of VOCs' destruction from industrial exhausts, particularly in the presence of Cl−VOCs.

3.8. Environmental Implications. Industrial emissions of waste gases usually involve multicomponent VOCs and, in some cases, are with trace amounts of chlorinated VOCs. This makes the applied catalysts suffer from severe deactivation and generate more toxic byproducts, particularly dioxins.[3] Herein, we developed a selective adsorption approach and fabricated a range of Ru-decorated SnO_2/CeO_2 catalysts. We showed that the Ru/SnCe-(5.8) catalyst was endowed with extraordinary H_2O and HCl resistances, with an excellent versatility for destructing a wide range of Cl−VOCs (e.g., m-CB, *o*-DCB, TCE, DCM, and ECH), routine VOCs (e.g., *N*-hexane, ethyl acetate, and toluene), and their mixtures. In particular, the fabricated monolithic catalyst by coating the Ru/SnCe-(5.8) powders onto a honeycomb ceramic has yielded a remarkable stability at 300 °C for m-CB destruction, with few dioxins being detected in the off-gas. Our work illustrates the efforts in transferring theoretical basis into realistic possibility and overcomes the bottlenecks of catalyst poisoning and secondary pollution in the catalytic destruction of multicomponent VOCs involving chlorinated organics.

■ ASSOCIATED CONTENT

Supporting Information

The Supporting Information is available free of charge at https://pubs.acs.org/doi/10.1021/acs.est.2c02925.

Catalyst characterizations; catalytic activity measurements; and BET, XRD, HRTEM, and XPS element analyses (PDF)

■ AUTHOR INFORMATION

Corresponding Authors

Qiguang Dai − *Key Laboratory for Advanced Materials, Research Institute of Industrial Catalysis, School of Chemistry and Molecular Engineering, East China University of Science and Technology, Shanghai 200237, P. R. China;* orcid.org/0000-0001-6764-6744; Email: daiqg@ecust.edu.cn

Xiaole Weng − *Key Laboratory of Environment Remediation and Ecological Health, Ministry of Education, College of Environmental and Resource Sciences, Zhejiang University, Hangzhou 310058, P. R. China; ZJU-Hangzhou Global Scientific and Technological Innovation Center, Hangzhou 311200, P. R. China;* orcid.org/0000-0003-2997-571X; Email: xlweng@zju.edu.cn

Authors

Yunpeng Long − *Key Laboratory of Environment Remediation and Ecological Health, Ministry of Education, College of Environmental and Resource Sciences, Zhejiang University, Hangzhou 310058, P. R. China*

Qingjie Meng − *School of Civil and Environmental Engineering, Ningbo University, Ningbo 315211, P. R. China*

Meiling Chen − *Key Laboratory of Environment Remediation and Ecological Health, Ministry of Education, College of Environmental and Resource Sciences, Zhejiang University, Hangzhou 310058, P. R. China*

Xueqing Luo − *ZJU-Hangzhou Global Scientific and Technological Innovation Center, Hangzhou 311200, P. R. China*

Hanfeng Lu − *College of Chemical Engineering, Zhejiang University of Technology, Hangzhou 310014, P. R. China*

Zhongbiao Wu − *Key Laboratory of Environment Remediation and Ecological Health, Ministry of Education, College of Environmental and Resource Sciences, Zhejiang University, Hangzhou 310058, P. R. China;* orcid.org/0000-0003-0182-5971

Complete contact information is available at: https://pubs.acs.org/10.1021/acs.est.2c02925

Author Contributions

All authors contributed to the development of the manuscript. All authors have approved the final version of the manuscript.

Notes

The authors declare no competing financial interest.

■ ACKNOWLEDGMENTS

This work was financially supported by the National Natural Science Foundation of China (grant no. 21922607), the Outstanding Youth Project of Zhejiang Natural Science Foundation (grant no. LR19E080004), and the Fundamental Research Funds for the Central Universities (no. 226-2022-00150). The authors also wanted to acknowledge Dr. Hehe Qian (ZJU-Hangzhou Global Scientific and Technological Innovation Center) for the help on HRTEM measurements, Chao Xi (Zhejiang Tianlan Environmental Protection Technology Co., Ltd.) for the monolithic-scale test and Yufeng Li from Shiyanjia Lab (www.shiyanjia.com) for the Raman analysis.

REFERENCES

(1) Guo, Y.; Wen, M.; Li, G.; An, T. Recent Advances in VOC Elimination by Catalytic Oxidation Technology onto Various Nanoparticles Catalysts: a Critical Review. *Appl. Catal., B* **2021**, *281*, 119447.

(2) He, C.; Cheng, J.; Zhang, X.; Douthwaite, M.; Pattisson, S.; Hao, Z. Recent Advances in the Catalytic Oxidation of Volatile Organic Compounds: a Review Based on Pollutant Sorts and Sources. *Chem. Rev.* **2019**, *119*, 4471−4568.

(3) Liu, J.; Dai, X.; Wu, Z.; Weng, X. Unveiling the Secondary Pollution in the Catalytic Elimination of Chlorinated Organics: The Formation of Dioxins. *Chin. Chem. Lett.* **2020**, *31*, 1410−1414.

(4) Yu, X.; Dai, L.; Deng, J.; Liu, Y.; Jing, L.; Zhang, X.; Gao, R.; Hou, Z.; Wei, L.; Dai, H. An Isotopic Strategy to Investigate the Role of Water Vapor in the Oxidation of 1, 2-dichloroethane over the Ru/WO_3 or Ru/TiO_2 Catalyst. *Appl. Catal., B* **2022**, *305*, 121037.

(5) Su, Y.; Fu, K.; Zheng, Y.; Ji, N.; Song, C.; Ma, D.; Lu, X.; Han, R.; Liu, Q. Catalytic Oxidation of Dichloromethane Over Pt-Co/HZSM-5 Catalyst: Synergistic Effect of Single-atom Pt, Co_3O_4, and HZSM-5. *Appl. Catal., B* **2021**, *288*, 119980.

(6) Liu, H.; Yang, J.; Jia, Y.; Wang, Z.; Jiang, M.; Shen, K.; Zhao, H.; Guo, Y.; Guo, Y.; Wang, L.; Dai, S.; Zhan, W. Significant Improvement of Catalytic Performance for Chlorinated Volatile Organic Compound Oxidation over RuOx Supported on Acid-Etched Co_3O_4. *Environ. Sci. Technol.* **2021**, *55*, 10734−10743.

(7) Weng, X.; Meng, Q.; Liu, J.; Jiang, W.; Pattisson, S.; Wu, Z. Catalytic Oxidation of Chlorinated Organics over Lanthanide Perovskites: Effects of Phosphoric Acid Etching and Water Vapor on Chlorine Desorption Behavior. *Environ. Sci. Technol.* **2019**, *53*, 884−893.

(8) Zhang, H.; Gao, X.; Gong, B.; Shao, S.; Tu, C.; Pan, J.; Wang, Y.; Dai, Q.; Guo, Y.; Wang, X. Catalytic combustion of CVOCs over MoOx/CeO_2 Catalysts. *Appl. Catal., B* **2022**, *310*, 121240.

(9) Yu, X.; Dai, L.; Peng, Y.; Deng, J.; Liu, Y.; Jing, L.; Zhang, X.; Hou, Z.; Wang, J.; Dai, H. High Selectivity to HCl for the Catalytic Removal of 1,2-Dichloroethane Over RuP/3DOM WOx: Insights into the Effects of P-Doping and H_2O Introduction. *Environ. Sci. Technol.* **2021**, *55*, 14906−14916.

(10) Chen, G.; Cai, Y.; Zhang, H.; Hong, D.; Shao, S.; Tu, C.; Chen, Y.; Wang, F.; Chen, B.; Bai, Y.; Wang, X.; Dai, Q. Pt and Mo Co-Decorated MnO_2 Nanorods with Superior Resistance to H_2O, Sintering, and HCl for Catalytic Oxidation of Chlorobenzene. *Environ. Sci. Technol.* **2021**, *55*, 14204−14214.

(11) Dai, Q.; Shen, K.; Deng, W.; Cai, Y.; Yan, J.; Wu, J.; Guo, L.; Liu, R.; Wang, X.; Zhan, W. HCl-Tolerant $HxPO_4$/RuOx−CeO_2 Catalysts for Extremely Efficient Catalytic Elimination of Chlorinated VOCs. *Environ. Sci. Technol.* **2021**, *55*, 4007−4016.

(12) Weng, X.; Sun, P.; Long, Y.; Meng, Q.; Wu, Z. Catalytic Oxidation of Chlorobenzene over $Mn_xCe_{1-x}O_2$/HZSM-5 Catalysts: A Study with Practical Implications. *Environ. Sci. Technol.* **2017**, *51*, 8057−8066.

(13) Dai, X.; Wang, X.; Long, Y.; Pattisson, S.; Lu, Y.; Morgan, D. J.; Taylor, S. H.; Carter, J. H.; Hutchings, G. J.; Wu, Z.; Weng, X. Efficient Elimination of Chlorinated Organics on a Phosphoric Acid Modified CeO_2 Catalyst: A Hydrolytic Destruction Route. *Environ. Sci. Technol.* **2019**, *53*, 12697−12705.

(14) Zhang, L.; Deng, W.; Cai, Y.; Dai, Q.; Guo, L. Comparative Studies of Phosphate-Modified CeO_2 and Al_2O_3 for Mechanistic Understanding of Dichloromethane Oxidation and Chloromethane Formation. *ACS Catal.* **2020**, *10*, 13109−13124.

(15) Ying, Q.; Liu, Y.; Li, H.; Zhang, Y.; Wu, Z. A Comparative Study of the Dichloromethane Catalytic Combustion over Ruthenium-based Catalysts: Unveiling the Roles of Acid types in Dissociative Adsorption and By-products Formation. *J. Colloid Interface Sci.* **2022**, *605*, 537−546.

(16) Gu, Y.; Shao, S.; Sun, W.; Xia, H.; Gao, X.; Dai, Q.; Zhan, W.; Wang, X. The Oxidation of Chlorinated Organic Compounds over W-modified Pt/CeO_2 Catalysts. *J. Catal.* **2019**, *380*, 375−386.

(17) Dai, Q.; Yin, L.-L.; Bai, S.; Wang, W.; Wang, X.; Gong, X.-Q.; Lu, G. Catalytic Total Oxidation of 1, 2-dichloroethane over VOx/CeO_2 Catalysts: Further Insights via Isotopic Tracer Techniques. *Appl. Catal., B* **2016**, *182*, 598−610.

(18) Fei, X.; Cao, S.; Ouyang, W.; Wen, Y.; Wang, H.; Wu, Z. A Convenient Synthesis of Core-shell Co_3O_4@ZSM-5 Catalysts for the Total Oxidation of Dichloromethane (CH_2Cl_2). *Chem. Eng. J.* **2020**, *387*, 123411.

(19) Lopezgranados, M.; Galisteo, F.; Lambrou, P.; Mariscal, R.; Sanz, J.; Sobrados, I.; Fierro, J.; Efstathiou, A. Role of P-containing Species in Phosphated CeO_2 in the Deterioration of Its Oxygen Storage and Release Properties. *J. Catal.* **2006**, *239*, 410−421.

(20) Ma, L.; Seo, C. Y.; Nahata, M.; Chen, X.; Li, J.; Schwank, J. W. Shape Dependence and Sulfate Promotion of CeO_2 for Selective Catalytic Reduction of NOx with NH_3. *Appl. Catal., B* **2018**, *232*, 246−259.

(21) Dai, Q.; Bai, S.; Wang, X.; Lu, G. Catalytic Combustion of Chlorobenzene over Ru-doped Ceria Catalysts: Mechanism Study. *Appl. Catal., B* **2013**, *129*, 580−588.

(22) Zhang, X.; Dai, L.; Liu, Y.; Deng, J.; Jing, L.; Yu, X.; Han, Z.; Zhang, K.; Dai, H. 3DOM CeO_2-supported Ru y M (M= Au, Pd, Pt) Alloy Nanoparticles with Improved Catalytic Activity and Chlorine-tolerance in Trichloroethylene Oxidation. *Catal. Sci. Technol.* **2020**, *10*, 3755−3770.

(23) Dai, Q.; Bai, S.; Wang, J.; Li, M.; Wang, X.; Lu, G. The Effect of TiO_2 Doping on Catalytic Performances of Ru/CeO_2 Catalysts during Catalytic Combustion of Chlorobenzene. *Appl. Catal., B* **2013**, *142*−*143*, 222−233.

(24) Mondelli, C.; Amrute, A. P.; Krumeich, F.; Schmidt, T.; Pérez-Ramírez, J. Shaped $RuO_2/SnO_2-Al_2O_3$ Catalyst for Large-Scale Stable Cl_2 Production by HCl Oxidation. *ChemCatChem* **2011**, *3*, 657−660.

(25) Seki, K. Development of RuO_2/rutile-TiO_2 Catalyst for Industrial HCl Oxidation Process. *Catal. Surv. Asia* **2010**, *14*, 168−175.

(26) Amrute, A. P.; Mondelli, C.; Schmidt, T.; Hauert, R.; Pérez-Ramírez, J. Industrial RuO_2-based Deacon Catalysts: Carrier Stabilization and Active Phase Content Optimization. *ChemCatChem* **2013**, *5*, 748−756.

(27) Crihan, D.; Knapp, M.; Zweidinger, S.; Lundgren, E.; Weststrate, C. J.; Andersen, J. N.; Seitsonen, A. P.; Over, H. Stable Deacon Process for HCl Oxidation over RuO_2. *Angew. Chem., Int. Ed.* **2008**, *47*, 2131−2134.

(28) Over, H.; Schomäcker, R. What Makes a Good Catalyst for the Deacon Process? *ACS Catal.* **2013**, *3*, 1034−1046.

(29) Hu, Z.; Liu, X.; Meng, D.; Guo, Y.; Guo, Y.; Lu, G. Effect of Ceria Crystal Plane on the Physicochemical and Catalytic Properties of Pd/ceria for CO and Propane Oxidation. *ACS Catal.* **2016**, *6*, 2265−2279.

(30) Sun, J. Q.; Wang, J. S.; Wu, X. C.; Zhang, G. S.; Wei, J. Y.; Zhang, S. Q.; Li, H.; Chen, D. R. Novel Method for High-yield Synthesis of Rutile SnO_2 Nanorods by Oriented Aggregation. *Cryst. Growth Des.* **2006**, *6*, 1584−1587.

(31) Gong, Y.; Liu, R.; Jiang, L.; Peng, A.; Xu, C.; Lu, X.; Ma, R.; Fu, Y.; Zhu, W.; Wang, S.; Zhou, L. Catalyst Development for HCl Oxidation to Cl_2 in the Fluorochemical Industry. *ACS Catal.* **2022**, *12*, 1098−1110.

(32) Yu, X.; Dai, L.; Deng, J.; Liu, Y.; Jing, L.; Zhang, X.; Jiang, X.; Hou, Z.; Wang, J.; Dai, H. Catalytic Performance and Intermediates Identification of Trichloroethylene Deep Oxidation over Ru/3DOM SnO_2 Catalysts. *J. Catal.* **2021**, *400*, 310−324.

(33) Wang, R.; Wang, Y.; Ren, M.; Sun, G.; Gao, D.; Chin Chong, Y. R.; Li, X.; Chen, G. Effect of Ceria Morphology on the Catalytic Activity of Ru/ceria for the Dehydrogenation of Ammonia Borane. *Int. J. Hydrogen Energy* **2017**, *42*, 6757−6764.

(34) Li, J.; Liu, Z.; Cullen, D. A.; Hu, W.; Huang, J.; Yao, L.; Peng, Z.; Liao, P.; Wang, R. Distribution and Valence State of Ru Species on CeO_2 Supports: Support Shape Effect and Its Influence on CO Oxidation. *ACS Catal.* **2019**, *9*, 11088−11103.

https://doi.org/10.1021/acs.est.2c02925
Environ. Sci. Technol. 2022, 56, 9762−9772

(35) Pouilloux, Y.; Autin, F.; Guimon, C.; Barrault, J. Hydrogenation of Fatty Esters over Ruthenium−tin Catalysts; Characterization and Identification of Active Centers. *J. Catal.* **1998**, *176*, 215−224.
(36) Ma, H.-Y.; Wang, G.-C. A First-Principles Study of the Mechanism and Site Requirements for CO_2 Methanation over CeO_2-Supported Ru Catalyst. *J. Phys. Chem. C* **2021**, *125*, 18161−18169.
(37) Guo, Y.; Mei, S.; Yuan, K.; Wang, D.-J.; Liu, H.-C.; Yan, C.-H.; Zhang, Y.-W. Low-Temperature CO_2 Methanation over CeO_2-Supported Ru Single Atoms, Nanoclusters, and Nanoparticles Competitively Tuned by Strong Metal−Support Interactions and H-Spillover Effect. *ACS Catal.* **2018**, *8*, 6203−6215.
(38) Jiang, F.; Wang, S.; Liu, B.; Liu, J.; Wang, L.; Xiao, Y.; Xu, Y.; Liu, X. Insights into the Influence of CeO_2 Crystal Facet on CO_2 Hydrogenation to Methanol over Pd/CeO_2 Catalysts. *ACS Catal.* **2020**, *10*, 11493−11509.
(39) Liu, Z.; Lu, Y.; Confer, M. P.; Cui, H.; Li, J.; Li, Y.; Wang, Y.; Street, S. C.; Wujcik, E. K.; Wang, R. Thermally Stable RuOx−CeO_2 Nanofiber Catalysts for Low-Temperature CO Oxidation. *ACS Appl. Nano Mater.* **2020**, *3*, 8403−8413.
(40) Sun, P.; Yu, H.; Liu, T.; Li, Y.; Wang, Z.; Xiao, Y.; Dong, X. Efficiently Photothermal Conversion in a MnO_x-based Monolithic Photothermocatalyst for Gaseous Formaldehyde Elimination. *Chin. Chem. Lett.* **2022**, *33*, 2564−2568.
(41) Fu, D.; Wu, X.; Cui, B.; Guo, Y.; Wang, H.; Han, J.; Ge, Q.; Zhu, X. $Ru_{0.05}Ce_{0.95}O_2$ Solid Solution Derived Ru Catalyst Enables Selective Hydrodeoxygenation of m-Cresol to Toluene. *ChemCatChem* **2021**, *13*, 4814−4823.
(42) Zhao, J.; Xi, W.; Tu, C.; Dai, Q.; Wang, X. Catalytic Oxidation of Chlorinated VOCs over Ru/Ti_xSn_{1-x} Catalysts. *Appl. Catal., B* **2020**, *263*, 118237.
(43) Satsuma, A.; Yanagihara, M.; Ohyama, J.; Shimizu, K. Oxidation of CO over Ru/Ceria Prepared by Self-dispersion of Ru Metal Powder into Nano-sized Particle. *Catal. Today* **2013**, *201*, 62−67.
(44) Wang, Z.; Huang, Z.; Brosnahan, J. T.; Zhang, S.; Guo, Y.; Guo, Y.; Wang, L.; Wang, Y.; Zhan, W. Ru/CeO_2 Catalyst with Optimized CeO_2 Support Morphology and Surface Facets for Propane Combustion. *Environ. Sci. Technol.* **2019**, *53*, 5349−5358.
(45) Dai, H.; Bell, A. T.; Iglesia, E. Effects of Molybdena on the Catalytic Properties of Vanadia Domains Supported on Alumina for Oxidative Dehydrogenation of Propane. *J. Catal.* **2004**, *221*, 491−499.
(46) Wang, D.; Huang, J.; Liu, F.; Xu, X.; Fang, X.; Liu, J.; Xie, Y.; Wang, X. Rutile RuO_2 Dispersion on Rutile and Anatase TiO_2 Supports: The Effects of Support Crystalline Phase Structure on the Dispersion Behaviors of the Supported Metal Oxides. *Catal. Today* **2020**, *339*, 220−232.
(47) Long, Y.; Su, Y.; Xue, Y.; Wu, Z.; Weng, X. V_2O5−WO_3/TiO_2 Catalyst for Efficient Synergistic Control of NO_x and Chlorinated Organics: Insights into the Arsenic Effect. *Environ. Sci. Technol.* **2021**, *55*, 9317−9325.
(48) Wang, W.; Tao, Y.; Wu, X.; Yang, L. Flower-like CeO_2-supported Small-sized Ru Nanoparticle Hybrids for Highly Efficient Alkaline Hydrogen Evolution: Roles of Interfacial Effects. *Appl. Surf. Sci.* **2022**, *581*, 152256.
(49) Wang, Y.-H.; Zheng, S.; Yang, W.-M.; Zhou, R.-Y.; He, Q.-F.; Radjenovic, P.; Dong, J.-C.; Li, S.; Zheng, J.; Yang, Z.-L.; Attard, G.; Pan, F.; Tian, Z.-Q.; Li, J.-F. In Situ Raman Spectroscopy Reveals the Structure and Dissociation of Interfacial Water. *Nature* **2021**, *600*, 81−85.
(50) Davis, J. G.; Gierszal, K. P.; Wang, P.; Ben-Amotz, D. Water Structural Transformation at Molecular Hydrophobic Interfaces. *Nature* **2012**, *491*, 582−585.
(51) Dai, Q.; Wu, J.; Deng, W.; Hu, J.; Wu, Q.; Guo, L.; Sun, W.; Zhan, W.; Wang, X. Comparative Studies of P/CeO_2 and Ru/CeO_2 Catalysts for Catalytic Combustion of Dichloromethane: From Effects of H_2O to Distribution of Chlorinated By-Products. *Appl. Catal., B* **2019**, *249*, 9−18.
(52) van den Brink, R. W.; Louw, R.; Mulder, P. Increased Combustion Rate of Chlorobenzene on Pt/γ-Al_2O_3 in Binary Mixtures with Hydrocarbons and with Carbon Monoxide. *Appl. Catal., B* **2000**, *25*, 229−237.

https://doi.org/10.1021/acs.est.2c02925
Environ. Sci. Technol. 2022, 56, 9762−9772